Photomodulation of transport in monolayer dichalcogenides

D. Meneses-Gustin, Luis Cabral, Matheus P. Lima, Juarez L. F. Da Silva, Emanuela Margapoti, Sergio E. Ulloa, Gilmar E. Marques, and Victor Lopez-Richard

Phys. Rev. B **98**, 241403 — Published 3 December 2018

DOI: 10.1103/PhysRevB.98.241403

Photo-modulation of transport in monolayer dichalcogenides

Diana Meneses-Gustin,[1] Luis A. Cabral,[1] Matheus P. Lima,[1] Juarez L. F. Da Silva,[2]
Emanuela Margapoti,[1] Sergio E. Ulloa,[3] Gilmar E. Marques,[1] and Victor Lopez-Richard[1]

[1]*Departamento de Física, Universidade Federal de São Carlos, 13565-905 São Carlos, SP, Brazil*
[2]*Instituto de Química de São Carlos, Universidade de São Paulo, 13560-970 São Carlos, São Paulo, Brazil*
[3]*Department of Physics and Astronomy and Ohio Materials Institute, Ohio University, Athens, OH 45701-2779, USA*

Surface functionalization emerges as an alternative pathway for electronic structure engineering in two-dimensional (2D) systems. We explore the hybrid heterostructure built from a 2D transition metal dichalcogenide atop a layer of photochromic self-assembled azobenzene molecules. This setup can modify carrier transport through the 2D nanosheet by an effective photoactived gating control, achieved through TRANS to CIS isomerization of the azobenzene in close contact with the 2D nanosheet. We show theoretically that this behavior can be ascribed to a tunable gating mechanism. We use a combination of atomistic calculations of the local effective potential profile with simulations of the electron scattering by such potential in a massive Dirac Hamiltonian formalism. We find that different isomers induce a local perturbation with drastically different features that explain well the experimental behavior.

Despite their success and importance in the electronics industry, bulk semiconductors currently used have some intrinsic drawbacks: they are rigid, have limited size shrink, and require the use of expensive processing technology. Thus, research efforts have recently shifted towards two-dimensional (2D) atomically thin crystals like graphene and transition-metal dichalcogenides (TMDs) that can be easily reduced to single layers through exfoliation or direct growth [1, 2]. These materials have the advantage of having low cost and high crystalline quality. Yet, unlike pristine graphene that lacks an energy gap, TMDs exhibit wide energy gaps in the visible or near infrared range of the spectrum and high electron mobility at room temperature [3, 4]. The high material quality and flexibility make these 2D crystals especially attractive for optoelectronic devices while holding the promise for the realization of new generation of storage devices, [5] solar cells [6], light detectors, and emitters [7, 8].

Of particular interest among TMDs is molybdenum disulfide, MoS_2, due to its indirect to direct gap transition upon reduction from bulk to a single layer, its photoluminescence and electro-luminescence in the visible range [9, 10], the possible strong valley polarization and high in-plane mobility. These features make it quite promising for the development of valleytronics applications and integrated circuit technologies [11, 12], ranging from flexible and transparent transistor devices, to low-power, high-efficiency biological and chemical sensing applications [13].

In these TMDs and related systems, the substrate plays an important role and can affect the observed properties by introducing defects and impurities and even inducing changes in the doping level [14, 15]. In particular, the combination of such 2D inorganic semiconductors with organic substrates has opened possibilities for new optoelectronic architectures [16–18].

In a previous work, Margapoti *et al.* presented the building blocks for photoswitchable gates, p-n diodes, and, potentially, optical transistors, by coupling MoS_2 monolayers and functionalized substrates with photochromic molecules [19, 20]. There, TMD sheets were

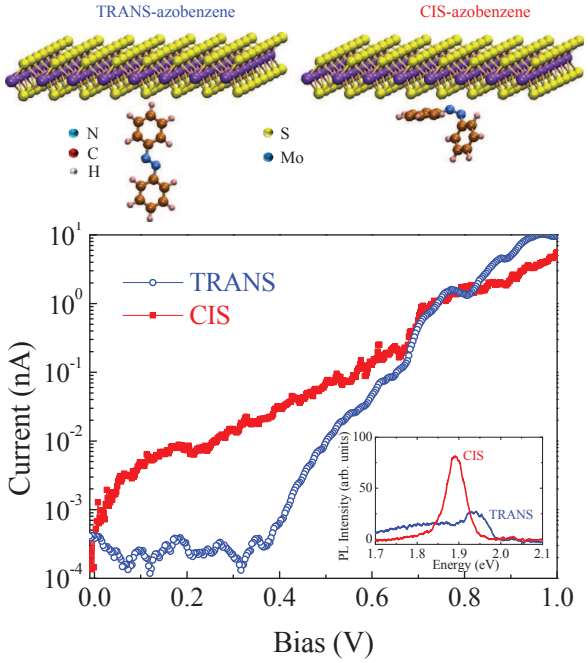

FIG. 1: Upper panels: atomistic representations of MoS_2 monolayer with and azobenzene molecule in its TRANS and CIS isomers. Spacer molecules not shown. Bottom panel: Current-voltage characteristics adapted from [19] (voltage zero is the turn-on value of the CIS configuration) obtained via conductive-atomic force microscopy for a heterostructure built from a single MoS_2 layer on top of self-assembled monolayer of photochromic azobenzene after UV (CIS) and white light exposure (TRANS). Current traces are obtained from a conductive tip atomic force microscope. The inset shows PL spectra recorded both in TRANS (blue spectrum) and in CIS (red spectrum) [20].

placed on top of a mixed self-assembled monolayer of spacer and azobenzene molecules, as represented in Fig. 1. To dilute the photochromic molecules, the substrate also contains spacer molecules, 6-(2-mercapto)-1-hexanol in a 1 : 1 ratio, to prevent aggregation and reduce steric hindrance for isomerization [19]. Such a procedure offers also the advantage of avoiding unintentional doping due to atom adsorption. The azobenzene molecules in the self-assembled layer can be made to switch isomerization through illumination with UV light, transitioning from their stable TRANS configuration to a metastable CIS form, represented in the upper panel of Fig. 1. The process is reversible using white light and leads to significant changes in the conductivity, as displayed in Fig. 1 [19]. The current-voltage characteristic were obtained using conductive-atomic force microscopy, following illumination procedures as reported before [21]. The optically-induced isomerization leads to a clear gating effect response for transport through the MoS_2 monolayer. The photoluminescence displayed in the inset of Fig. 1(c) [20], is also strongly suppressed in the TRANS configuration, turning bright after the CIS transition.

The main goal of this paper is to explore the nature of these effects and provide a microscopic description of how the different isomers interact with the 2D TMD. For this purpose, a thorough atomistic characterization of the substrate-monolayer interaction has been obtained from *ab initio* simulations. These subsequently allow the parametrization and description of the electron scattering in the conduction band by the potential induced by the isomerization.

The microscopic characterization of the induced potentials on the MoS_2 layer by the different isomers allows us to understand the general behavior of experimental c-AFM traces presented in Fig. 1, as arising from an effective gating on the dichalcogenide monolayer. This local interaction creates scattering potentials that would naturally affect electronic transport in such sample. We present a theoretical calculation of the resulting cross-section for such perturbations in a Dirac Hamiltonian description which would result in the modulation of the mean free times for the electrons in the system according to the isomerization configuration of the azobenzene molecule. The resulting mobility is then predicted to change substantially upon isomerization. The contrasting induced perturbations on the TMD produced by the different isomerizations and their effect on transport are in general agreement with experimental observations.

Two geometrical conformations depicted in the upper panels of Fig. 1 were considered for azobenzene molecules interacting with a single layer of MoS_2. Both configurations were fully relaxed using state-of-the-art *ab initio* calculations based on the density functional theory (DFT) [22, 23], employing the Perdew-Burke-Ernzerhof (PBE) exchange-correlation functional [24]. The MoS_2 monolayer is simulated with a supercell of 128 S and 64 Mo atoms.

The D3 van der Waals correction [25] was employed to improve the description of the long range interactions. The Kohn-Sham equations were solved using the Projected Augmented Wave (PAW) method [26, 27] as implemented in the Vienna *ab initio* Simulation Package (VASP) [28, 29]. The valence states considered are $5s^1 4d^5$, $3s^2 3p^4$, $2s^2 2p^2$, $2s^2 2p^3$, and $1s^1$ for Mo, S, C, N, and H, respectively. A plane wave cutoff energy of 473 eV was employed, 12.5% larger than recommended in VASP. For the Brillouin zone integration, only the Γ-point was used to sample the reciprocal space, and the atoms were allowed to relax until all forces became smaller than 0.01 eV/Å. The characterization of the molecule adsorption on the MoS_2 surface under 13 configurations can be found in Ref. 30 and its Supplementary Material while two additional arrangements have been tested here and presented in Ref. 31. The discussion has been focused on the lower energy conformation.

Figure 2(a), depicts the calculated electronic local density of states (LDOS) for azobenzene adsorbed on a MoS_2 single layer, in TRANS and CIS configurations. This density of states is projected onto all the sites of a given chemical species. Note that the valence and conduction bands in this range are mainly localized at the Mo sites, indicating that the transport channels affected by the absorbed azobenzene are mostly localized on the plane passing through Mo atoms. The LDOS projected on the molecule exhibits sharp peaks, demonstrating weak hybridization between the states of the molecule and the substrate, typical of the van der Waals bonding. Indeed, since the azobenzene/layer interaction is a local effect, the LDOS for the Mo and S species, which is normalized by the number of the involved atoms in the monolayer, is practically unaffected by the molecule isomerization condition.

To understand the strong modulation driven by the light-induced isomerization of azobenzene, it is essential to note that the TRANS configuration has a C-H bond pointing to the substrate, as seen in Fig. 1. On the other hand, in its CIS isomerization, the N-N group is nearest the substrate. This leads to two contrasting environments defining the molecule/layer interaction. Due to the electronegativity difference between the C-H and N-N groups, the molecular isomerization (TRANS or CIS) results in a modulation of the local electrostatic potential, which directly affects the transport measurements.

In order to quantify these concepts, we present the charge distribution induced by the azobenzene/layer interaction in panels (c) and (d) of Fig. 2. For TRANS azobenzene, the surface interaction results in an electron accumulation at the nearby S layer, indicated by the blue isosurface in Fig. 2(c). On the other hand, for the CIS isomer, the proximity of the N-N group to the monolayer results in an accumulation of holes close to the S surface, as indicated in Fig. 2(d). Thus, the TRANS or CIS

configurations induce charge accumulation with opposite sign on the MoS_2 layer, mostly due to the electronegativity difference between the N-N and the C-H groups. Such charge accumulation generates a perturbation in the local electrostatic potential, which can be seen as the source of the current and PL modulation depicted in Fig. 1.

The electrostatic potential perturbation (ΔV) generated by the presence of the azobenzene molecules, can be evaluated as

$$\Delta V(\mathbf{r}) = V_{mol/layer}(\mathbf{r}) - V_{layer}(\mathbf{r}) - V_{mol}(\mathbf{r}), \qquad (1)$$

where $V_{mol/layer}$ is the electrostatic potential of the system composed by a molecule adsorbed on a MoS_2 layer. V_{layer} (V_{mol}) is the electrostatic potential of an isolated MoS_2 layer (isolated molecule), with the atomic positions fixed exactly as in the geometry used to calculate $V_{mol/layer}$. This avoids spurious perturbations in the potential envelope, generated by differences in the atomic positions. The vacuum energy was set to zero for all electrostatic potentials. We calculated the vacuum level from the average electrostatic potential in the region of the simulation box which is far from the MoS_2 layer, and where it becomes constant.

Since the states around the Fermi energy are mostly composed of Mo atomic orbitals (see Fig. 2(a)), the most relevant region for the characterization of $\Delta V(\mathbf{r})$ is the plane defined by Mo atoms. The calculated profile of $\Delta V(\mathbf{r})$ along this plane, in the region near the molecule, is shown in Fig. 2(b) (3D profiles are provided in Ref. 31). It is worth noting the contrasting configurations of ΔV on the izomerization of the azobenzene. The TRANS configuration generates a repulsive profile bump in ΔV. On the other hand, the CIS configuration induces an attractive potential well. These are consistent with the sign of the charge induced by the azobenzene isomers in Fig. 2(c) and (d). With this information, we now proceed to estimate the effect of such potential perturbation on the in-plane carrier scattering.

By using scattering theory, we consider electronic transport within the MoS_2 monolayer locally perturbed by the presence of scattering centers created by the azobenzene SAM. The profile is emulated by a cylindrical potential defined by

$$\Delta V(\mathbf{r}) = \begin{cases} V & \text{for } r \leq L \\ 0 & \text{for } r > L, \end{cases} \qquad (2)$$

that defines either an attractive or repulsive perturbation according to the sign of V and can be parameterized with the values obtained from the atomistic simulation just discussed. In contrast to Ref. 32, the scalar representation of the perturbation is possible here since the scattering centers result from molecule clusters, much larger than the interatomic distance in the TMD.

In turn, the Hamiltonian that describes the electronic structure in this transition metal dichalcogenide monolayer is [12]

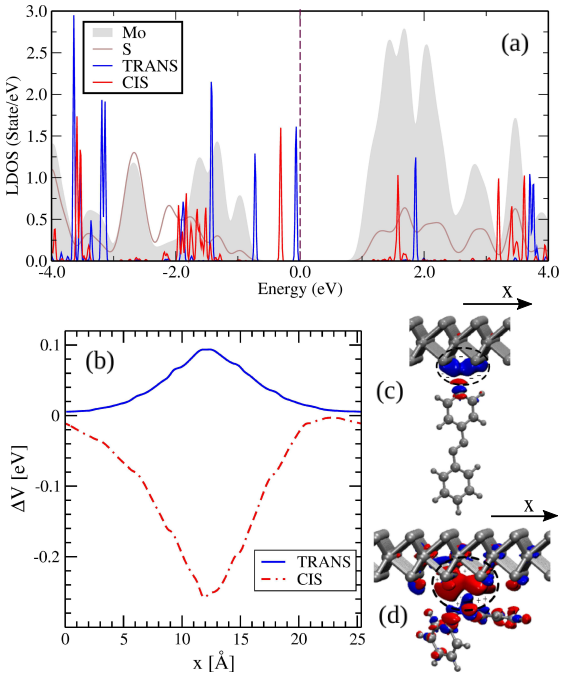

FIG. 2: (a) LDOS aligned by the vacuum level for both TRANS and CIS AZO-molecules interacting with the MoS_2 layers, as depicted in Fig. 1. Blue and red solid lines represent the DOS summed over the azobenzene molecule (H, C, N) atoms, in the TRANS and CIS orientations, respectively. For each curve, the DOS is normalized by the number of atoms. States with negative energies are occupied. (b) Electrostatic potential perturbation, ΔV, generated by the adsorption of azobenzene molecules on the MoS_2 surface. Charge density dislocations, $\Delta\rho = \rho_{mol/layer} - \rho_{layer} - \rho_{mol}$, for (c) TRANS and (d) CIS isomers. The labels *mol/layer*, *mol* and *layer* represent systems composed by the azobenzene adsorbed on the MoS_2 layer, isolated azobenzene, and isolated layer, respectivelly. The red (blue) isosurface represents 0.002e (−0.002e).

$$H_D = at(\tau q_x \sigma_x + q_y \sigma_y) + \frac{\Delta}{2}\sigma_z - \tau\lambda\frac{\sigma_z - 1}{2}s_z, \qquad (3)$$

where a is the MoS_2 in-plane lattice constant, t the effective hopping integral, $\tau = \pm 1$ represents the valley index, σ_i are Pauli matrices that act on the spinor space corresponding to the two Mo-orbitals in a hexagonal lattice, Δ is the hybridization that produces the optical gap, 2λ denotes the spin splitting at the valence band due to spin-orbit coupling, and s_z is the Pauli matrix for spin. The scattering problem is then tackled searching for solutions ψ satisfying $[H_D + V(\mathbf{r})]\,\psi = E\psi$, as described in Ref. 33.

The size of the scattering centers in this system was determined experimentally in Ref. 21, within the range 70-90 Ådue to clustering of the azobenzene molecules. Thus, we simulated the probability density for $V = -0.2$eV, and $V = 0.2$eV for $L = 70$Å, shown in Fig. 3(a) and

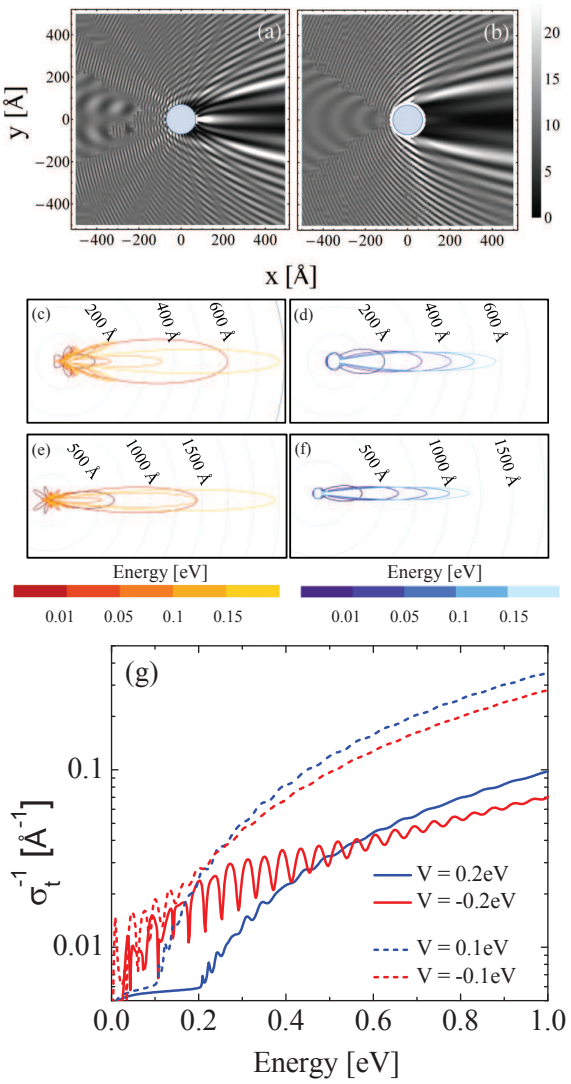

FIG. 3: Probability density of a scattered function for (a) attractive potential ($V = -0.2$ eV), and (b) repulsive potential ($V = 0.2$ eV) with $L = 70$ Å, and incident energy of 0.3 eV. (c) - (f) Differential cross section as function of the scattering angle for various values of incident electron energy: (c) and (d), with $L = 70$ Å, for an attractive, $V = -0.2$ eV, and repulsive, $V = 0.2$ eV, potentials, respectively; (d) and (e) analogous to (c) and (d), but for $L = 100$ Å. (g) Calculated inverse transport scattering cross section as a function of incident energy for repulsive and attractive potentials with $L = 70$ Å.

(b), respectively. The following parameters were used for MoS_2: $a = 3.193$Å, $t = 1.10$eV, $\Delta = 1.66$eV, and $2\lambda = 0.15$eV [12]. In Fig. 3(a) we note a bright area behind the attractive scattering center; in contrast, the barrier case results in a shadow appearing in the same place. This sharp contrast in the forward scattering amplitude is also visible at all energies, as we will see below. To better characterize the scattering patterns, we calculate the differential scattering cross section. Correspondingly, the probability density to find scattered electrons along a given direction is given by [34]

$$\frac{d\sigma}{d\theta} = |f_q(\theta)|^2. \tag{4}$$

Figure 3(c) and (d) show the differential cross section (4) displayed as polar plots for attractive and repulsive potentials for various values of the incident energy and $L = 70$ Å. The angular dependence of the scattering is clearly different from the barrier to well case and is also sensitive to the potential spatial width, as seen in the results of Fig. 3(e) and (f), where $L = 100$ Å (note the different polar scales). The forward scattering increases as the energy grows in all cases, but grows faster for attractive potentials giving rise to the difference seen in Fig. 3(a) and (b). This will impact the mean free path for collisions, proportional to the mean free time, that ultimately modulates the current. [35] In order to relate the fraction of electrons flowing along the system with an experimentally measurable quantity, we use the transport cross section to estimate the mean free time τ_t [34], proportional to the mobility, $\tau_t = 1/(n_{imp} v_f \sigma_t)$, with the transport cross section defined by (in the diluted regime)

$$\sigma_t = \int_{-\pi}^{\pi} d\theta \, \frac{d\sigma}{d\theta} \, (1 - \cos\theta), \tag{5}$$

where n_{imp} is the scattering center concentration, and v_f the Fermi velocity. Thus, the transport ability of the system can be characterized by the quantity $\sigma_t^{-1}(E)$. This can be correlated to the profiles generated according to the isomerization condition of the adsorbed molecule and their clusters.

For both, barrier and well cases, the inverse transport cross section is shown in Fig. 3(g). High and low current flux states can be tuned according to the relative size of barrier and well perturbations. Two sets of barrier heights and well depths have been assessed for $L = 70$ Å to elucidate these trends. Note in the case of repulsive V that once the energy of the incoming electrons exceeds the barrier height, the mobility grows much faster than before. This may be correlated to the current onset displayed in Fig. 1 for the TRANS configuration above $V = 0.3$ V. We emphasize that a direct comparison is not possible, as the electrically-active region in the experiment is somewhat ill-defined. In turn, for an attractive potential, corresponding to the CIS isomerization, oscillations appear due to the presence of resonant states [33]. The absence of these features in the experiment can be ascribed to the irregular shape of the effective scattering potentials, as well as the low coherence at finite temperature.

It is clear that the qualitative correspondence with the experimental current displayed in Fig. 1 depends in detail on the strength of the molecule-layer interaction that modulates the height, shape and depth of the scattering

potential. These features will depend strongly on the specifics of azobenzene to spacer molecule ratio values, as well as the overall geometrical characteristics of the sample.

Thus, the gating of the the MoS_2 layer, which is affected by the relative distance and electronegativity of the species involved in the molecule-layer interaction, can indeed induce contrasting transport states under certain conditions. It is also expected that given the lower mobility of carriers, this may promote an enhancement of the probability of electron-hole pair recombination. This may lead to an increase of the PL intensity, especially with azobenzene in the CIS configuration, as seen in the inset of Fig. 1(c).

In summary, we have characterized a hybrid inorganic-organic nanostructure with responsivity at wavelengths of light that induce TRANS and CIS configurations of photochromic azobenzene molecules. Based on these results, it is possible to conclude that the photo-gating mechanism can be ascribed to the charge redistribution that takes place locally at the proximity region between the azobenzene and the MoS_2 sheet. According to the isomers available, this interaction may lead to either an attractive or a repulsive potential. This affects both the electron flux, and subsequently the conductance, and charge trapping, tuning the luminescence.

The authors are grateful for financial support by the Brazilian Agencies FAPESP (grants $2014/19142-2$, $2015/16175-0$, $2016/02065-0$, and $2014/02112-3$), CNPq, CAPES and USNSF DMR/508325, and NSF grant DMR 1508325 (Ohio).

[1] W. K. Park, Y. Yoon, Y. H. Song, S. Y. Choi, S. Kim, Y. Do, J. Lee, H. Park, D. H. Yoon. and W. S. Yang, Sci. Rep.-UK **7**, 16414 (2017).
[2] M. J. Crane, M. B. Lim, X. Zhou, and P. J. Pauzauskie, Microsystems and Nanoengineering **3**, 17032 (2017).
[3] B. Radisavljevic, A. Radenovic, J. Brivio, V. Giacometti, and A. Kis, Nature Nanotech. **6**, 147 (2011).
[4] H. Fang, S. Chuang, T. C. Chang, K. Takei, T. Takahashi, and A. Javey, Nano Lett. **12**, 3788 (2012).
[5] K. Leng, Z. Chen, X. Zhao, W. Tang, B. Tian, C. T. Nai, W. Zhou, and K. P. Loh, ACS Nano **10**, 9208 (2016).
[6] A. Pospischil, M. M. Furchi, and T. Mueller, Nature Nanotec. **9**, 257 (2014).
[7] R. S. Sundaram, M. Engel, A. Lombardo, R. Krupke, A. C. Ferrari, Ph. Avouris, and M. Steiner, Nano Lett. **13**, 1416 (2013).
[8] A. Nurbawono and C. Zhang, Appl. Phys. Lett. **103**, 203110 (2013).
[9] D. Sercombe, S. Schwarz, O. Del Pozo-Zamudio, F. Liu, B. J. Robinson, E. A. Chekhovich, I. I. Tartakovskii, O. Kolosov, and A. I. Tartakovskii, Sci. Rep.-UK **3**, 3489 (2013).
[10] A. V. Kolobov and J. Tominaga. *Two-Dimensional Transition-Metal Dichalcogenides*, vol. 239 Springer Series in Materials Science (Springer International Publishing, Cham, 2016).
[11] A. K. M. Newaz, D. Prasai, J. I. Ziegler, D. Caudel, S. Robinson, R. F. Haglund Jr., and K. I. Bolotin, Solid State Commun. **155**, 49 (2013).
[12] D. Xiao, G.-B. Liu, W. Feng, X. Xu, and W. Yao, Phys. Rev. Lett. **108**, 196802 (2012).
[13] I. Song, C. Park, and H. C. Choi, RSC Adv. **5**, 7495 (2015).
[14] M. Buscema, G. A. Steele, H. S. J. van der Zant, and A. Castellanos-Gomez, Nano Res. **7**, 1 (2014).
[15] J. Feng, X. Qian, C.-W. Huang, and J. Li, Nature Photonics **6**, 866 (2012).
[16] R. Schlesinger, F. Bianchi, S. Blumstengel, C. Christodoulou, R. Ovsyannikov, B. Kobin, K. Moudgil, S. Barlow, S. Hecht, S.R. Marder, F. Henneberger, and N. Koch, Nature Comm. **6**, 6754 (2015).
[17] X. Liu, J. Gu, K. Ding, D. Fan, X. Hu, Y.-W. Tseng, Y.-H. Lee, V. Menon, and S. R. Forrest, Nano Lett. 17 (5), 3176 (2017).
[18] D. Jariwala, T. J. Marks, and M. C. Hersam, Nature Mat. **16**, 170 (2017).
[19] E. Margapoti, J. Li, O. Ceylan, M. Seifert, F. Nisic, T. Le Anh, F. Meggendorfer, C. Dragonetti, C.-A. Palma, J. V. Barth, and J. J. Finley, Adv. Mater. **27**, 1426 (2015).
[20] J. Li, J. Wierzbowski, O. Ceylan, J. Klein, F. Nisic, T. L. Anh, F. Meggendorfer, C.-A. Palma, C. Dragonetti, J. V. Barth, J. J. Finley, and E. Margapoti, Appl. Phys. Lett. **105**, 241116 (2014).
[21] E. Margapoti, P. Strobel, M. M. Asmar, M. Seifert, J. Li, M. Sachsenhauser, O. Ceylan, C.-A. Palma, J. V. Barth, J. A. Garrido, A. Cattani-Scholz, S. E. Ulloa, and J. J. Finley, Nano Lett. **14**, 6823 (2014).
[22] P. Hohenberg and W. Kohn. Phys. Rev. **136**, 864 (1964).
[23] W. Kohn and L. J. Sham, Phys. Rev. **140**, 1133 (1965).
[24] J. P. Perdew, K. Burke, and M. Ernzerhof, Phys. Rev. Lett. **77**, 3865 (1996).
[25] S. Grimme, J. Antony, S. Ehrlich, and H. Krieg, J. Chem. Phys. **132**, 154104 (2010).
[26] P. E. Blochl, Phys. Rev. B **50**, 17953 (1994).
[27] G. Kresse and D. Joubert, Phys. Rev. B **59**, 1758 (1999).
[28] T. Bučko, J. Hafner, S. Lebegue, and J. G. Ángyán, J. Phys. Chem. A **114**, 11814 (2010).
[29] J. Moellmann and S. Grimme, Phys. Chem. Chem. Phys. **12**, 8500 (2010).
[30] L. Cabral, F. P. Sabino, M. P. Lima, G. E. Marques, V. Lopez-Richard, and J. L. F. Da Silva, J. Phys. Chem. C **122**, 18895 (2018).
[31] See Supplemental Material at [URL will be inserted by publisher] for details on the DFT characterization of the adsorption process.
[32] F. J. dos Santos, D. A. Bahamon, R. B. Muniz, K. McKenna, E. V. Castro, J. Lischner, and A. Ferreira, Phys. Rev. B **98**, 081407(R) (2018).
[33] D. Meneses-Gustin, S. E. Ulloa, and V. Lopez-Richard, Phys. Rev. B **98**, 125301 (2018).
[34] M. M. Asmar and S. E. Ulloa, Phys. Rev. B **91**, 165407 (2015).
[35] A. A. Stabile, A. Ferreira, J. Li, N. M. R. Peres, and J. Zhu Phys. Rev. B **92**, 121411(R) (2015).